A Note on the Depth of Sidelobe Contamination in Acoustic Doppler Current Profiles

S. J. LENTZ,[a] A. KIRINCICH,[a] AND A. J. PLUEDDEMANN[a]

[a] *Physical Oceanography, Woods Hole Oceanographic Institution, Woods Hole, Massachusetts*

ABSTRACT: Acoustic Doppler current profilers (ADCP) do not provide reliable water velocity measurements near the sea surface or bottom because acoustic sidelobe reflections from the boundary contaminate the Doppler velocity measurements. The apparent depth of the center of the sidelobe reflection is $z_{sl} = h_a[1 - \cos(\theta)]$, where h_a is the distance from the ADCP acoustic head to the sea surface and θ is the ADCP beam angle. However, sidelobe contamination extends one and a half ADCP bins below z_{sl} as the range gating of the acoustic return causes overlap between adjacent ADCP bins. Consequently, the contaminated region $z < z_{sl} + 3\Delta z/2$ is deeper than traditionally suggested, with a dependence on bin size Δz. Direct observations confirming both the center depth of the sidelobe reflection and the depth of contamination are presented for six bottom-mounted, upward-looking ADCPs. The sidelobe reflection is isolated by considering periods of weak wind stresses when the sea surface is smooth and there is nearly perfect reflection of the main beams away from the ADCP and hence little acoustic return from the main beams to the ADCP.

KEYWORDS: Acoustic measurements/effects; Data processing/distribution; Profilers, oceanic

1. Introduction

Acoustic Doppler current profilers (ADCP) do not provide reliable water velocity measurements near the sea surface or bottom because acoustic sidelobe reflections from the boundary contaminate the Doppler velocity measurements (Appell et al. 1991). Even though the acoustic sidelobes are much weaker than the main beams (e.g., Appell et al. 1991; Gordon 1996), the surface reflection is ~40 dB (or 100 times) stronger than from particles in the water. Consequently, sidelobe reflections from the surface can be as strong as the main beam returns from the water column. As a result, acoustic returns from the main beams are only useful for calculating currents prior to the arrival of the vertical sidelobe reflection from the sea surface (Appell et al. 1991; Gordon 1996). From the ADCP beam geometry (Fig. 1) the height above the acoustic head coinciding to the arrival of the vertical sidelobe reflection is $h_{sl} = h_a \cos(\theta)$, where h_a is the distance from the ADCP acoustic head to the sea surface and θ is the ADCP beam angle from vertical (typically 20° or 25°). The corresponding depth below the surface of the sidelobe reflection is

$$z_{sl} = h_a - h_{sl} = h_a[1 - \cos(\theta)]. \tag{1}$$

For a 20° beam angle "this means data from the last 6% of the range to the surface can be contaminated" (Gordon 1996).

Experience indicates that sidelobe contamination extends farther below the sea surface than z_{sl}, often by a factor of 2 (e.g., Appell et al. 1991; Teague et al. 2001) Yet there is no consistent criteria for determining the near-surface region

contaminated by the sidelobe reflection and a percentage of the range to the surface greater than 6% is often used (e.g., Kirincich et al. 2005; Fewings et al. 2008; Kirincich and Lentz 2017). The extension of the sidelobe contamination below z_{sl} is commonly attributed to the effects of surface gravity waves, as their time-varying surface reflections are normally smeared over a number of depth bins within the ensemble averaging normally employed with ADCP sampling. However, below we show that the contaminated region extends below z_{sl} even in the absence of surface gravity waves.

Here we show that sidelobe contamination extends below z_{sl} because z_{sl} is the depth of the center of the sidelobe reflection which can be anywhere in a range cell and the triangular weight function of the acoustic return overlaps adjacent depth cells (Gordon 1996). The sidelobe surface reflections are strong enough to contaminate the range cell below the one containing the center of the sidelobe reflection (Appell et al. 1991; Plimpton et al. 2004). To be explicit let Δz be the vertical extent of each range cell and z_i be the depth of the center of the ith range cell below the sea surface. The top of each range cell is at $z_i - \Delta z/2$ The center of the sidelobe reflection is contained in the deepest range cell where the top of the range cell is above z_{sl}, that is, $z_i - \Delta z/2 > z_{sl}$. Since the range cell just below this one is also contaminated, because of the acoustic return overlap between cells, the range cells contaminated by sidelobe reflection are from (1):

$$z_{ic} < h_a[1 - \cos(\theta)] + 3\Delta z/2. \tag{2}$$

The key point is that the near-surface depth range contaminated by sidelobe reflection extends deeper than the center of the sidelobe reflection and depends not only on the beam angle and sea surface height above the ADCP head, but also the bin size (Appell et al. 1991; Plimpton et al. 2004). The following analysis is based on commonly used ADCPs with

---
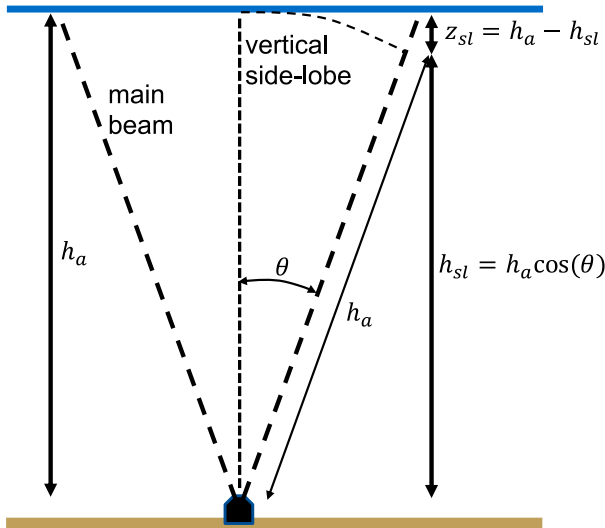
FIG. 1. Geometry of the ADCP beams and depth of sidelobe surface reflection contamination.
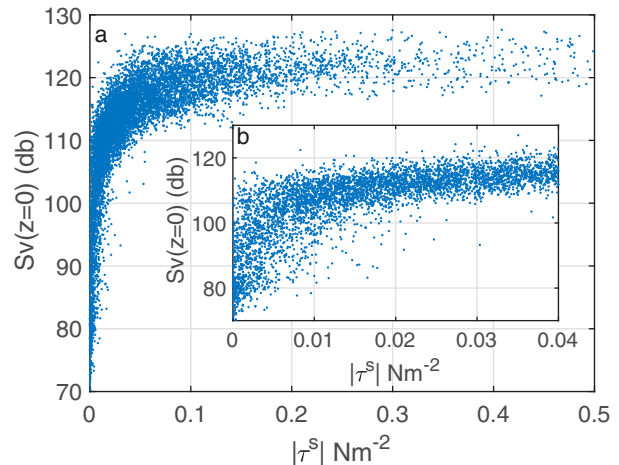

FIG. 2. Acoustic backscatter from the depth bin identified as the sea surface vs wind stress from one of the 600-kHz ADCPs for (a) all collected data and (b) only small wind stress magnitudes. The reduced backscatter from the sea surface at small wind stresses is due to a glassy sea surface causing the main beam energy to be reflected away from the ADCP.

piston transducers and transducer size varying with frequency to produce a similar beam pattern (Appell et al. 1991; Gordon 1996). In this case, ADCP frequency has minimal impact on sidelobe contamination. The results may not apply for ADCPs with significantly different transducer size or geometry for a given frequency.

2. Measurements and processing

To demonstrate that (1) is an estimate of the center of sidelobe reflection and that contamination extends to the depth given by (2), measurements are analyzed from six upward-looking ADCPs deployed on bottom frames south of Martha's Vineyard, Massachusetts, from June to December 2014 (Kirincich and Lentz 2017). The ADCPs were deployed in water depths of 14–26 m. The instruments were RDI 1200- or 600-kHz ADCPs with four beams oriented 20° from vertical measuring currents and acoustic return profiles with 0.5-m (1200 kHz) or 1-m (600 kHz) vertical bins. The ADCPs also measured pitch, roll, pressure, and temperature at the instrument. The ADCPs sampled at 0.33 to 1 Hz and analyses were done on 30-min averages.

Bottom pressures were measured using SeaBird Seagauges equipped with accurate Paroscientific quartz pressure gauges mounted on the ADCP platforms. The Paroscientific pressure gauges have an estimated accuracy equivalent to a few millimeters of seawater (Lentz et al. 1999), far more accurate than the ADCP pressure gauges and much smaller than the ADCP bin size. Strings of five to seven SeaBird Microcat temperature–conductivity instruments spanning the water column on surface moorings deployed next to the ADCPs provided sound absorption and density profile estimates. Meteorological measurements are from the Martha's Vineyard Coastal Observatory Air–Sea Interaction Tower 2.8 km offshore. Wind stress is estimated using the Coupled Ocean–Atmosphere Response Experiment (COARE) 3.5 bulk algorithm (Edson et al. 2013).

See Kirincich and Lentz (2017) for more details on the instrument array and measurements.

Acoustic backscatter (Sv) in units of dB was estimated from the acoustic returns by correcting for beam spreading and sound absorption (e.g., Visbeck and Fischer 1995; Deines 1999). The ambient acoustic noise is not known so the absolute magnitude of the backscatter estimates have an unknown offset (Gostiaux and van Haren 2010) that will vary with for example wind speed (Visbeck and Fischer 1995). Current and acoustic backscatter profiles were transformed to a surface following coordinate frame with an overresolved vertical spacing of 0.1 m using estimates of sea surface height relative to the fixed ADCP. Sea surface height variations on time scales of 30 min and longer were estimated using the hydrostatic relationship and the measurements of bottom pressure, atmospheric pressure, and density profiles.

3. Results

The sidelobe reflection from the sea surface can be isolated by assuming that during very weak winds, the sea surface is smooth or glassy. With no surface roughness to reflect the energy of the main acoustic beam back to the transducer, the main beam can experience nearly perfect reflection off the surface and away from the ADCP. If the acoustic return from the main beam is weak enough, the strongest return will be from the vertical sidelobe that is reflected directly back to the instrument. With the sea surface determined, to an accuracy of a few centimeters from the pressure and density measurements, two criteria are used to isolate times when the acoustic return at the surface might be dominated by the vertical sidelobe reflection: low wind stress magnitudes $|\tau^s| < 0.02$ N m^{-2} (based on Fig. 2, results are similar for all six sites) and weak acoustic backscatter from the sea surface [$Sv(z = 0) < 80$ dB for 600-kHz ADCPs or $Sv(z = 0) < 65$ dB for 1200-kHz
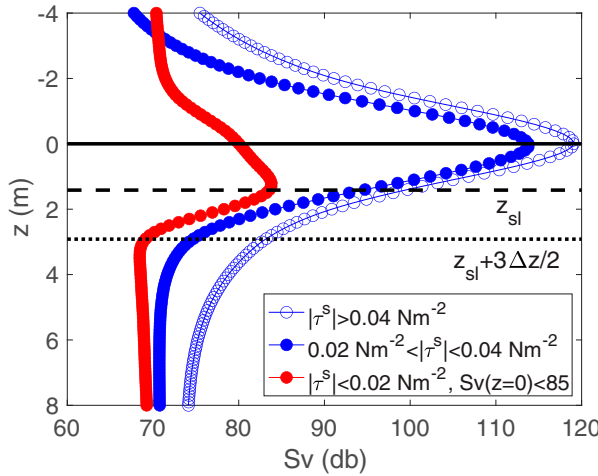
FIG. 3. Mean acoustic backscatter as a function of depth below sea surface from one of the 600-kHz ADCPs. For wind stress magnitudes greater than 0.02 N m^{-2} the maximum backscatter occurs at the sea surface ($z = 0$) as expected for the ADCP main beams. However, for small wind stress magnitudes (<0.02 N m^{-2}) and weaker acoustic backscatter at $z = 0$ (red symbols), the maximum acoustic backscatter occurs below the surface at the depth predicted for vertical sidelobe reflection from the sea surface [Eq. (1)].
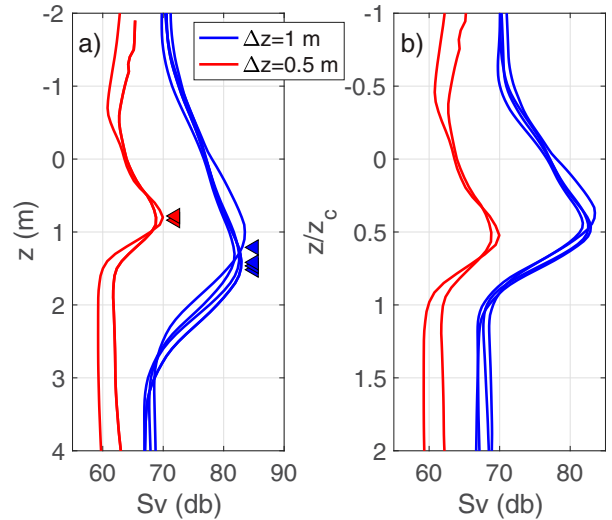

FIG. 4. Illustrating the effect of bin size on z_{sl}, the average acoustic backscatter profiles for sidelobe reflections from the surface (weak winds and low acoustic backscatter from surface) vs (a) depth below sea surface and (b) depth normalized by z_c from Eq. (2) for two 1200-kHz ADCPs with 0.5-m bins (red), and four 600-kHz ADCPs with 1-m bins (blue). Triangles in (a) mark the depth of z_{sl} determined from Eq. (1).

ADCPs] because the sidelobe is about 30–40 dB weaker than the main beams (Appell et al. 1991). The latter criteria proved to be a much stronger constraint, accounting for less than 3% of the profiles (note the wide range of Sv for $|\tau^s| < 0.02$ N m^{-2} in Fig. 2b).

An example of average backscatter profiles near the sea surface for one of the 600-kHz ADCPs is shown in Fig. 3. When $|\tau^s| < 0.02$ N m^{-2} the maximum backscatter is relatively large and centered at $z = 0$, as expected for main beam reflection off the sea surface (blue open and closed circles). When $|\tau^s| < 0.02$ N m^{-2} and Sv($z = 0$) < 80 dB the maximum backscatter is at the expected apparent depth of the center of the vertical sidelobe reflection z_{sl} given by Eq. (1) (Fig. 3, red circles). There is similar agreement for all six ADCPs between the observed and predicted "apparent" depth of the center of the sidelobe reflection (Table 1, Fig. 4a). This confirms that z_{sl} is an accurate estimate of the apparent depth of the center of the vertical sidelobe sea surface reflection.

TABLE 1. For six ADCP sites: depth of ADCP head h_a, ADCP vertical bin length Δz, observed z_{sl}^{obs} and predicted z_{sl} apparent depth of sidelobe reflection, and predicted depth of sidelobe contamination $z_c = z_{sl} + 3\Delta z/2$. Units are m. ADCP beam angle is 20°.

h_a	Δz	z_{sl}^{obs}	z_{sl}	z_c
13.9	0.5	0.8	0.8	1.6
25.1	1.0	1.4	1.5	3.0
13.0	0.5	0.8	0.8	1.5
24.3	1.0	1.3	1.5	3.0
23.5	1.0	1.4	1.4	2.9
20.1	1.0	1.1	1.2	2.7

More importantly, for weak winds ($|\tau^s| < 0.04$ N m^{-2}), the backscatter anomaly associated with the sea surface extends to the depth $z_c = z_{sl} + 3\Delta z/2$ given by (2), well below the center of the sidelobe reflection (Fig. 3, solid red and blue circles). For larger wind stresses (Fig. 3, open blue circles), the anomaly near the sea surface extends deeper than z_c, likely due to both increased surface gravity wave variability and injection of air bubbles associated with whitecapping. Normalizing the depth by z_c collapses the profiles for all six ADCPs so the anomaly associated with the sidelobe reflection from the sea surface is above $z/z_c = 1$ (Fig. 4b). This confirms that the acoustic return from the sidelobe reflections off the sea surface extends to the depth z_c given by (2). Standard data quality parameters, beam correlation, percent good, and error velocity all exhibit similar vertical structures in relation to z_c (not shown). Beam correlation and percent good are anomalously low between z_c and the surface with a transition to high values below z_c. Error velocity is anomalously high between z_c and the surface with a transition to low values below z_c.

Another, more direct, indication of contamination of the Doppler current profiles by the sidelobe surface reflection is a dramatic increase in the magnitude of the bin-to-bin velocity shear magnitude. Standard deviations of the bin-to-bin velocity shear are small and approximately uniform with depth below z_c and then increase substantially toward the surface above z_c (Fig. 5b). Standard deviations of the bin-to-bin velocity shears above z_c are too large to be caused by wind-driven shear (e.g., Fig. 5a, dashed line). Standard deviations of the vertical shear in the estimated surface gravity wave Stokes velocity or the Eulerian Stokes–Coriolis velocity (estimated following Lentz et al.
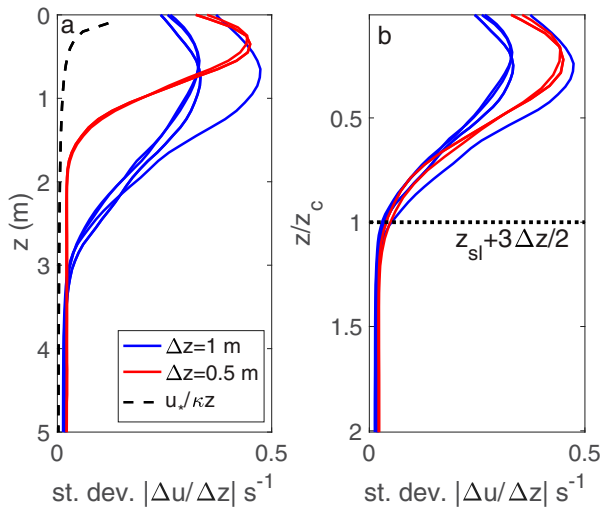
FIG. 5. Standard deviation of magnitude of current shear vs (a) depth below sea surface and (b) depth below surface normalized by $z_c = z_{sl} + 3\Delta z/2$ for all six moorings. The standard deviations are for entire deployment. For comparison the standard deviation of the predicted wind-driven shear is also shown [dashed line in (a)]. The wind-driven shear standard deviations are estimated from the Air–Sea Interaction Tower wind stress time series assuming law of the wall ($\partial u/\partial z = u_*/\kappa z$, where $u_* = \sqrt{|\tau^s|/\rho}$).
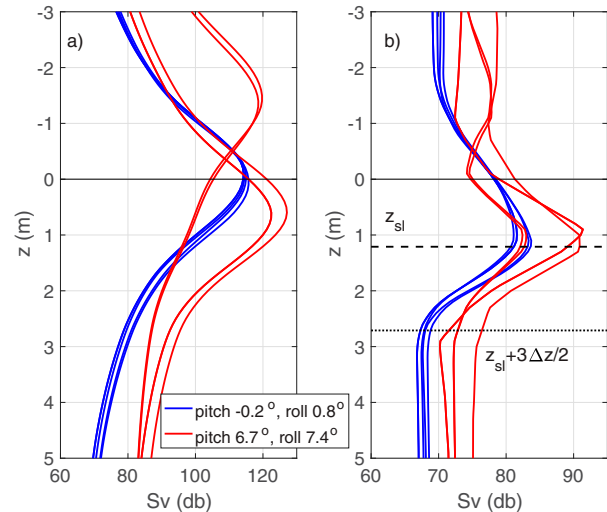

FIG. 6. Average acoustic backscatter from each of the four beams of a 600-kHz ADCP with depth for (a) main beams (wind stress was greater than 0.04 N m^{-2}), and (b) sidelobes [wind stress was less than 0.02 N m^{-2} and acoustic backscatter (Sv) from surface ($z = 0$) was less than 80 or 90 dB]. Two deployments are shown (blue and red), illustrating the effects of pitch and roll on acoustic returns of the main beam, but not the sidelobe.

2008) at these sites (not shown) are even smaller than the wind-driven shear standard deviations. There is also no reason the depth of the sudden increase in velocity shear should depend on ADCP bin size or frequency (cf. red and blue lines, Fig. 5a) if it was due to a physical process. The deeper transition for the ADCPs with 1-m bins relative to the ADCPs with 0.5-m bins is consistent with Eq. (2) and the additional dependence on bin size (cf. Figs. 5a,b).

4. Discussion and summary

A challenge in estimating the depth of sidelobe contamination using (2) is accurate estimation of h_a, the distance from the ADCP head to the sea surface. The analysis presented here used very accurate Paroscientific Quartz pressure sensors, atmospheric pressure, and density profiles to estimate sea surface height. Biases of ±20 cm between these sea surface height estimates and acoustic sea surface height estimates from the ADCP during moderate to strong wind stresses were removed. Using the less accurate ADCP pressure gauges without including water density or atmospheric pressure variations results in time-varying inaccuracies in the sea surface height estimates of typically tens of centimeters or more. This is due in part to an uncorrected temperature dependence in most ADCP pressure gauges. Estimating sea surface height directly from the ADCP acoustic returns (e.g., Visbeck and Fischer 1995) is more direct but is noisy, requires accurate estimates of sound speed throughout the water column, and is not reliable at low wind speeds when the sea surface is smooth because of uncertainty in the relative contribution of the sidelobe reflection and the

weaker return from the main beam. The vertical beam on the newer five-beam ADCPs provides a more accurate estimate of the sea surface height (particularly if there are accurate estimates of sound speed throughout the water column).

Instrument tilt (pitch and roll) does not directly impact the vertical extent of the sidelobe contamination. This is because the sidelobe is broad (see beam patterns in Appell et al. 1991; Gordon 1996), in contrast to the narrow main beams, and the acoustic return from the sidelobe is dominated by the vertical portion of the sidelobe that is reflected directly back to the ADCP. This is clearly seen in two deployments of one of the ADCPs at the same site. During the first deployment the pitch and roll were small ($-0.2°$ and $0.8°$, respectively). During most of the second deployment the pitch and roll were larger ($6.7°$ and $7.4°$) because of an abrupt shift in the bottom frame shortly after deployment. During the first deployment the maximum acoustic return is at the sea surface ($z = 0$) for all four beams, as expected for small pitch and roll (Fig. 6a, blue lines). During the second deployment the maximum acoustic return is apparently above the sea surface for two of the beams because the beam angle is greater than 20° due to the pitch and roll and below the sea surface for the two beams with angles less than 20° due to the pitch and roll (Fig. 6a, red lines). In contrast, the sidelobe reflections are maximum at the same, expected depth z_{sl}, for all four beams during both deployments (Fig. 6b, blue and red lines). Additionally for all four beams during both deployments the sidelobe acoustic return anomaly associated with the sea surface occurs above $z_{sl} + 3\Delta z/2$. However, if the bin heights are remapped to account for the pitch and roll (e.g., Ott 2002), then the location of the center of the sidelobe reflection given by (1) will depend on the different angles for each beam associated with the pitch and roll.

Surface gravity waves should increase the region contaminated by sidelobe reflection because the sea surface will be closer to the ADCP under the wave troughs than indicated by the average sea surface height. However, it was not possible to isolate the sidelobe reflection when waves were large because this almost always occurred during strong wind stresses and hence the sea surface was rough. The injection of air bubbles associated with whitecapping can also makes it difficult to identify the base of the acoustic return anomaly associated with the sea surface reflection.

In summary, reliable current measurements from upward looking acoustic Doppler current profilers are limited to depths bin below $z_{sl} + 3\Delta z/2$ because of sidelobe reflections, where z_{sl} is the center depth of the sidelobe reflection given by (1) and Δz is the ADCP bin size. Consequently the near-surface depth range contaminated by sidelobe reflection depends on the ADCP bin size, as well as the beam angle and sea surface height above the ADCP. ADCP observations masked just using z_{sl} would have biased estimates of currents in the top one to two bins as a result of incorrect identification of the sidelobe contaminated area. These results, and Eq. (2), should also apply to downward-looking ADCP deployments, although the potentially large range of tilt variability in ship mounted instruments will cause additional complications to ensemble-averaged ADCP results.

REFERENCES

Appell, G. F., P. D. Bass, and M. A. Metcalf, 1991: Acoustic Doppler current profiler performance in near surface and bottom boundaries. *IEEE J. Oceanic Eng.*, **16**, 390–396, https://doi.org/10.1109/48.90903.

Deines, K. L., 1999: Backscatter estimation using broadband acoustic Doppler current profilers. *Proc. Sixth Working Conf. on Current Measurement*, San Diego, CA, IEEE, 249–253, https://doi.org/10.1109/CCM.1999.755249.

Edson, J. B., and Coauthors, 2013: On the exchange of momentum over the open ocean. *J. Phys. Oceanogr.*, **43**, 1589–1610, https://doi.org/10.1175/JPO-D-12-0173.1.

Fewings, M., S. J. Lentz, and J. Fredericks, 2008: Observations of cross-shore flow driven by cross-shore winds on the inner continental shelf. *J. Phys. Oceanogr.*, **38**, 2358–2378, https://doi.org/10.1175/2008JPO3990.1.

Gordon, R. L., 1996: Acoustic Doppler current profiler: Principles of operation—A practical primer. Teledyne RD Instruments Rep., 52 pp.

Gostiaux, L., and H. van Haren, 2010: Extracting meaningful information from uncalibrated backscattered echo intensity data. *J. Atmos. Oceanic Technol.*, **27**, 943–949, https://doi.org/10.1175/2009JTECHO704.1.

Kirincich, A. R., and S. J. Lentz, 2017: The importance of lateral variability on exchange across the inner shelf south of Martha's Vineyard, MA. *J. Geophys. Res. Oceans*, **122**, 2360–2381, https://doi.org/10.1002/2016JC012491.

——, J. A. Barth, B. A. Grantham, B. A. Menge, and J. Lubchenco, 2005: Wind-driven inner-shelf circulation off central Oregon during summer. *J. Geophys. Res.*, **110**, C10S03, https://doi.org/10.1029/2004JC002611.

Lentz, S., R. T. Guza, S. Elgar, F. Feddersen, and T. H. C. Herbers, 1999: Momentum balances on the North Carolina inner shelf. *J. Geophys. Res.*, **104**, 18 205–18 226, https://doi.org/10.1029/1999JC900101.

——, M. Fewings, P. Howd, J. Fredericks, and K. Hathaway, 2008: Observations and a model of undertow over the inner continental shelf. *J. Phys. Oceanogr.*, **38**, 2341–2357, https://doi.org/10.1175/2008JPO3986.1.

Ott, M. W., 2002: An improvement in the calculation of ADCP velocities. *J. Atmos. Oceanic Technol.*, **19**, 1738–1741, https://doi.org/10.1175/1520-0426(2002)019<1738:AIITCO>2.0.CO;2.

Plimpton, P. E., H. P. Freitag, and M. J. McPhaden, 2004: Processing of subsurface ADCP data in the equatorial Pacific. NOAA Tech. Memo. OAR PMEL-125, 41 pp.

Teague, C. C., J. F. Vesecky, and Z. R. Hallock, 2001: A comparison of multifrequency HF radar and ADCP measurements of near-surface currents during COPE-3. *IEEE J. Oceanic Eng.*, **26**, 399–405, https://doi.org/10.1109/48.946513.

Visbeck, M., and J. Fischer, 1995: Sea surface conditions remotely sensed by upward-looking ADCPs. *J. Atmos. Oceanic Technol.*, **12**, 141–149, https://doi.org/10.1175/1520-0426(1995)012<0141:SSCRSB>2.0.CO;2.